Supplement of

Impacts of anthropogenic aerosols on a snowfall event – A case study in the Guanzhong Basin and its surrounding areas, China

Yuning Yang et al.

Correspondence to:
Naifang Bei (bei.naifang@mail.xjtu.edu.cn) and Guohui Li (ligh@ieecas.cn)

S1. WRF-Chem model

The WRF-Chem model (Version 3.5) (Grell et al., 2005) with modifications by Li et al. (2010, 2011a, 2011b) has been applied to quantitatively evaluate the aerosol effect on a short-time heavy rainfall event in Guanzhong Basin (GZB). The model includes a new flexible gas phase chemical module and the CMAQ aerosol module developed by US EPA (Binkowski & Roselle, 2003). For the aerosol simulations, the CMAQ/models-3 aerosol module (AERO5) has been incorporated into the model. In this aerosol component, the particle size distribution is represented as the superposition of three lognormal sub-distributions, called modes. The processes of coagulation, particles growth by the addition of mass, and new particle formation are included. The new particle production rate due to binary nucleation of H_2SO_4 and water vapor is parameterized following Kulmala et al. (1998). The wet deposition is based on the method in the CMAQ module and the dry deposition of chemical species followed Wesely (1989). The photolysis rates are calculated using the Fast Tropospheric Ultraviolet and Visible (FTUV) Radiation Model with the aerosol and cloud effects on photolysis (Li et al., 2005, 2011a).

ISORROPIA (version 1.7) is used to predict the thermodynamic equilibrium between the ammonia-sulfate-nitrate-chloride-water aerosols and their gas phase precursors of H_2SO_4-HNO_3-NH_3-HCl-water vapor (Nenes et al., 1998). The organic aerosol (OA) module is based on the volatility basis-set (VBS) approach with aging; detailed information can be found in Li et al. (2011b). The primary OA (POA) components from traffic-related combustion and biomass burning emissions are represented by nine surrogate species with saturation concentrations (C*) ranging from 10^{-2} to 10^{6} μg m^{-3} at room temperature (Shrivastava et al., 2008), and assumed to be semi-volatile and photochemically reactive (Robinson et al., 2007). The secondary OA (SOA) formation from each anthropogenic or biogenic precursor is calculated using four semi-volatile VOCs with effective saturation concentrations of 1, 10, 100, and 1000 μg m^{-3} at 298 K. The SOA formation via the heterogeneous reaction of glyoxal and methylglyoxal is parameterized as a first-order irreversible uptake by aerosol particles and cloud droplets with an uptake coefficient of 3.7×10^{-3} (Liggio et al., 2005, Volkamer et al., 2007, Zhao et al., 2006).

S2. Aerosol radiative module

In the present study, Goddard shortwave module developed by Chou and Suarez (1999) and Chou et al. (2001) is employed to account for the ARI effect on particulate matter (PM) pollution and the FTUV module

(Li et al., 2005; 2011a) is used to consider the API effect. The aerosol radiative module developed by Li et al. (2011a) has been incorporated into the WRF-Chem model to calculate the aerosol optical depth (AOD or $\boldsymbol{\tau_a}$), single scattering albedo (SSA or $\boldsymbol{\omega_a}$), and the asymmetry factor ($\boldsymbol{g_a}$).

In the CMAQ aerosol module, aerosols are represented by a three-moment approach with a lognormal size distribution:

$$\boldsymbol{n(lnD)} = \frac{N}{\sqrt{2\pi}\boldsymbol{ln\sigma_g}}\boldsymbol{exp}[-\frac{1}{2}(\frac{\boldsymbol{lnD-lnD_g}}{\boldsymbol{ln\sigma_g}})^2] \quad (1)$$

Where D is the particle diameter, N is the number distribution of all particles in the distribution, D_g is the geometric mean diameter, and σ_g is the geometric standard deviation. To calculate the aerosol optical properties, the aerosol spectrum is first divided into 48 bins from 0.002 to 25.0 μm, with radius r_i. The aerosols are classified into four types: (1) internally mixed sulfate, nitrate, ammonium, hydrophilic organics and black carbon (BC), and water; (2) hydrophobic organics; (3) hydrophobic BC; and (4) other unidentified aerosols (generally dust-like aerosols). These four kinds of aerosols are assumed to be mixed externally. For the internally mixed aerosols, the complex refractive index at a certain wavelength (λ) is calculated based on the volume-weighted average of the individual refractive index. Given the particle size and complex refractive index, the extinction efficiency (Q_e), ω_a and g_a are calculated using the Mie theory at a certain wavelength (λ). The look-up tables of Q_e, ω_a and g_a are established according to particle sizes and refractive indices to avoid multiple Mie scattering calculation. The aerosol optical parameters are interpolated linearly from the look-up tables with the calculated refractive index and particle size in the module.

The $\boldsymbol{\tau_a}$ at a certain $\boldsymbol{\lambda}$ in a given atmospheric layer $\boldsymbol{k}$ is determined by the summation over all types of aerosols and all bins:

$$\boldsymbol{\tau_a(\lambda,k)} = \sum_{i=1}^{48}\sum_{j=1}^{4}\boldsymbol{Q_e}\,\boldsymbol{(\lambda,r_i,j,k)\pi r_i^2 n(r_i,j,k)\Delta Z_k} \quad (2)$$

Where $\boldsymbol{n(r_i,j,k)}$ is the number concentration of $\boldsymbol{j}$-th kind of aerosols in the $\boldsymbol{i}$-th bin. $\boldsymbol{\Delta Z_k}$ is the depth of an atmospheric layer. The weighted-mean values of $\boldsymbol{\omega_a}$ and $\boldsymbol{g_a}$ are then calculated by using D'Almeida et al. (1991):

$$\boldsymbol{\omega_a(\lambda,k)} = \frac{\sum_{i=1}^{48}\sum_{j=1}^{4}\boldsymbol{Q_e(\lambda,r_i,j,k)\pi r_i^2 n(r_i,j,k)\omega_a(r_i,j,k)\Delta Z_k}}{\sum_{i=1}^{48}\sum_{j=1}^{4}\boldsymbol{Q_e(\lambda,r_i,j,k)\pi r_i^2 n(r_i,j,k)\Delta Z_k}} \quad (3)$$

$$\boldsymbol{g_a(\lambda,k)} = \frac{\sum_{i=1}^{48}\sum_{j=1}^{4}\boldsymbol{Q_e(\lambda,r_i,j,k)\pi r_i^2 n(r_i,j,k)\omega_a(r_i,j,k)g_a(\lambda,r_i,j,k)\Delta Z_k}}{\sum_{i=1}^{48}\sum_{j=1}^{4}\boldsymbol{Q_e(\lambda,r_i,j,k)\pi r_i^2 n(r_i,j,k)\omega_a(r_i,j,k)\Delta Z_k}} \quad (4)$$

When the wavelength-dependent $\boldsymbol{\tau_a}$, $\boldsymbol{\omega_a}$, and $\boldsymbol{g_a}$ are calculated, they can be used in the Goddard shortwave module to evaluate the ARI effect and the FTUV to evaluate the API effect. The aerosol refractive indices used for Mie scattering calculation are listed in Table S2. In the base case simulation of the Base scenario, the BC aging from the hydrophobic to the hydrophilic state occurs at a pseudo first order rate of 9.26×10^{-5} s^{-1} (Moffet and Prather, 2009) during daytime and 7.10×10^{-6} s^{-1} (Cooke and Wilson, 1996) during nighttime. As suggested by Moffet and Prather (2009), the effective density is 0.7 g cm^{-3} for fresh BC and 1.8 g cm^{-3} for aged BC to consider the variation of the BC morphology. In order to take into account absorption of brown carbon (BrC) observed by Barnard et al. (2008) in Megacities, the imaginary refractive index of POA measured by Kirchstetter et al. (2004) is employed in the present study (Table S2). Detailed information can be found in Li et al. (2011a).

S3. Aerosol-cloud interactions module

A two-moment bulk microphysics scheme with aerosol effects developed by Morrison et al. (2009) is utilized to account for aerosol-cloud interactions (ACI) in the simulation. The mass mixing ratio and number concentration of five hydrometeors are predicted in the bulk microphysics scheme, including cloud water, rain water, ice crystal, snow flake, and graupel. The Gamma function is used to represent the size distribution of the five hydrometeors. Detailed information is provided in Morrison et al. (2009).

The aerosol activation to cloud condensation nuclei (CCN) and ice nuclei (IN) is based on the CMAQ/models3 aerosol module (Binkowski and Roselle, 2003). Aerosols are simulated in the CMAQ using a modal approach assuming that particles are represented by three superimposed log-normal size distributions. The aerosol species, including sulfate, nitrate, ammonium, POA, SOA, BC, and other unidentified species (dust-like) are predicted in the module.

For the CCN nucleation, the critical radius of dry aerosols is calculated from the *k*-Köhler theory developed by Petters and Kreidenweis (2007; 2008; 2013) using water vapor supersaturation predicted by the model (Yau and Rogers, 1989; Pruppacher and Klett, 1997). If the activated CCN radius is less than 0.03 μm, the mass of water condensation on CCN is calculated under the equilibrium assumption; otherwise, the mass of water condensing on CCN is calculated by $\boldsymbol{m_w = K\frac{4}{3}\pi r_a^3 \rho_w}$ at zero supersaturation, where $3 < K < 8$ (Khain, 2009). Additionally, a novel, flexible approach, proposed by Philips et al. (2008; 2013) is used to parameterize the ice heterogeneous nucleation within clouds. The method has empirically derived

dependencies on the chemistry and surface area of multiple species of IN aerosols, mainly including dust, black and organic carbon aerosols. Three kinds of ice nucleation mechanisms are considered in the method, including contact, immersion, and condensation freezing. Detailed information can be found in Zhou et al. (2017).

S4. Statistical methods

In the present study, the mean bias (*MB*), root mean square error (*RMSE*), the index of agreement (*IOA*), and correlation efficient (*R*) are used as indicators to evaluate the performance of WRF-Chem model in simulations against measurements. *IOA* describes the relative difference between the model and observation, ranging from 0 to 1, with 1 indicating perfect agreement.

$$\boldsymbol{MB} = \frac{\mathbf{1}}{\boldsymbol{N}}\sum_{\boldsymbol{i}=\mathbf{1}}^{\boldsymbol{N}}(\boldsymbol{P_i} - \boldsymbol{O_i}) \tag{5}$$

$$\boldsymbol{RMSE} = \left[\frac{\mathbf{1}}{\boldsymbol{N}}\sum_{\boldsymbol{i}=\mathbf{1}}^{\boldsymbol{N}}(\boldsymbol{P_i} - \boldsymbol{O_i})^{\mathbf{2}}\right]^{\frac{\mathbf{1}}{\mathbf{2}}} \tag{6}$$

$$\boldsymbol{IOA} = \mathbf{1} - \frac{\sum_{\boldsymbol{i}=\mathbf{1}}^{\boldsymbol{N}}(\boldsymbol{P_i}-\boldsymbol{O_i})^{\mathbf{2}}}{\sum_{\boldsymbol{i}=\mathbf{1}}^{\boldsymbol{N}}(|\boldsymbol{P_i}-\overline{\boldsymbol{O}}|+|\boldsymbol{O_i}-\overline{\boldsymbol{O}}|)^{\mathbf{2}}} \tag{7}$$

$$\boldsymbol{R} = \frac{\sum_{\boldsymbol{i}=\mathbf{1}}^{\boldsymbol{N}}[(\boldsymbol{P_i}-\overline{\boldsymbol{P}})\times(\boldsymbol{O_i}-\overline{\boldsymbol{O}})]}{\sqrt{\sum_{\boldsymbol{i}=\mathbf{1}}^{\boldsymbol{N}}(\boldsymbol{P_i}-\overline{\boldsymbol{P}})^{\mathbf{2}}\times\sum_{\boldsymbol{i}=\mathbf{1}}^{\boldsymbol{N}}(\boldsymbol{O_i}-\overline{\boldsymbol{O}})^{\mathbf{2}}}} \tag{8}$$

Where $\boldsymbol{P_i}$ and $\boldsymbol{O_i}$ are the predicted and observed pollutant concentrations, respectively. *N* is the total number of the predictions used for comparisons, and $\overline{\boldsymbol{P}}$ and $\overline{\boldsymbol{O}}$ represents the average of the prediction and observation, respectively.

In order to evaluate the overall response of clouds or cloud systems to the changes in aerosols, involved with the chemical composition, the concentration, or the representation approach, the statistics of a given model variable, e.g., the mean value averaged over the entire domain or a specific region and throughout the integration period or a particular interval, is much more meaningful than the instant distribution of this variable at a given time step. Therefore, the population mean (*p-mean* hereinafter) of a given variable over all qualified grid points and for a given integration interval is used in the study, which is defined as:

$$\overline{\boldsymbol{c}}^{\boldsymbol{p}} = \frac{\mathbf{1}}{\sum_{\boldsymbol{t}=\boldsymbol{T_1}}^{\boldsymbol{T_2}}\sum_{\substack{\boldsymbol{q}>\boldsymbol{q_{min}}\\ \boldsymbol{n}>\boldsymbol{n_{min}}}}\Delta\boldsymbol{z}(\vec{\boldsymbol{r}},\boldsymbol{t})}\sum_{\boldsymbol{t}=\boldsymbol{T_1}}^{\boldsymbol{T_2}}\sum_{\substack{\boldsymbol{q}>\boldsymbol{q_{min}}\\ \boldsymbol{n}>\boldsymbol{n_{min}}}}\boldsymbol{c}(\vec{\boldsymbol{r}},\boldsymbol{t})\Delta\boldsymbol{z}(\vec{\boldsymbol{r}},\boldsymbol{t}) \tag{9}$$

Where *c* represents a given quantity. The calculation using Equation (9) only applies to the grid points where both the mass concentration *q* and number concentration *n* of a hydrometeor or the summation of several

hydrometeors exceed their given minima. Δz is the vertical grid spacing. T_1 and T_2 are the start and end output time steps, respectively.

125

References

Barnard, J. C., Volkamer, R., and Kassianov, E. I.: Estimation of the mass absorption cross section of the organic carbon component of aerosols in the Mexico City Metropolitan Area, Atmos. Chem. Phys., 8, 6665-6679, doi:10.5194/acp-8-6665-2008, 2008.

Binkowski, F. S. and Roselle, S. J.: Models-3 community multiscale air quality (CMAQ) model aerosol component 1. Model description, J. Geophys. Res.-Atmos., 108, doi:10.1029/2001jd001409, 2003.

Chen, F. and Dudhia, J.: Coupling an advanced land surface–hydrology model with the Penn State–NCAR MM5 modeling system. Part I: Model implementation and sensitivity, Mon. Weather Rev., 129, 569-585, doi:10.1175/1520-0493(2001)129<0569:CAALSH>2.0.CO;2, 2001.

Chou, M. D. and Suarez, M. J.: A solar radiation parameterization for atmospheric studies, in: Technical Report Series on Global Modeling and Data Assimilation (NASA/TM-1999-104606), edited by Suarez M. J., Goddard Space Flight Center, Greenbelt, Maryland, 15, 1999.

Chou, M. D., Suarez, M. J., Liang, X. Z., Yan, M. M. H., and Cote, C.: A thermal infrared radiation parameterization for atmospheric studies, in: Technical Report Series on Global Modeling and Data Assimilation (No. NASA/TM-2001-104606), edited by Suarez M. J., Goddard Space Flight Center, Greenbelt, Maryland, 19, 2001.

Cooke, W. F. and Wilson, J. J.: A global black carbon aerosol model, J. Geophys. Res.-Atmos., 101, 19395-19409, doi:10.1029/96jd00671, 1996.

D'Almeida, G. A., Koepke, P., and Shettle, E. P.: Atmospheric aerosols: global climatology and radiative characteristics, J. Med. Microbiol., 54, 55-61, 1991.

Grell, G. A. and Dévényi, D.: A generalized approach to parameterizing convection combining ensemble and data assimilation techniques, Geophys. Res. Lett., 29, 38-1, doi:10.1029/2002GL015311, 2002.

Grell, G. A., Peckham, S. E., Schmitz, R., McKeen, S. A., Frost, G., Skamarock, W. C., and Eder, B.: Fully coupled "online" chemistry within the WRF model, Atmos. Environ., 39, 6957-6975, doi:10.1016/j.atmosenv.2005.04.027, 2005.

Guenther, A., Karl, T., Harley, P., Wiedinmyer, C., Palmer, P. I., and Geron, C.: Estimates of global terrestrial isoprene emissions using MEGAN (Model of Emissions of Gases and Aerosols from Nature), Atmos. Chem. Phys., 6, 3181-3210, doi:10.5194/acp-6-3181-2006, 2006.

Horowitz, L. W., Walters, S., Mauzerall, D. L., Emmons, L. K., Rasch, P. J., Granier, C., Tie, X., Lamarque, J-F., Schultz, M. G., Tyndall, G. S., Orlando, J. J., and Brasseur, G. P.: A global simulation of tropospheric ozone and related tracers: Description and evaluation of MOZART, version 2, J J. Geophys. Res.-Atmos., 108, doi:10.1029/2002JD002853, 2003.

Janić, Z. I.: Nonsingular implementation of the Mellor-Yamada level 2.5 scheme in the NCEP Meso model, Office note (National Centers for Environmental Prediction (U.S.)) ; 437, https://repository.library.noaa.gov/view/noaa/11409, 2001.

Kirchstetter, T. W., Novakov, T., and Hobbs, P. V.: Evidence that the spectral dependence of light absorption by aerosols is affected by organic carbon, J. Geophys. Res.-Atmos., 109, doi:10.1029/2004jd004999, 2004.

Kulmala, M., Laaksonen, A., and Pirjola, L.: Parameterizations for sulfuric acid/water nucleation rates, J. Geophys. Res.-Atmos., 103, 8301-8307, doi:10.1029/97JD03718, 1998.

Li, G., Zhang, R., Fan, J., and Tie, X.: Impacts of black carbon aerosol on photolysis and ozone, J. Geophys. Res.-Atmos., 110, D23206, doi:10.1029/2005JD005898, 2005.

Li, G., Lei, W., Zavala, M., Volkamer, R., Dusanter, S., Stevens, P., and Molina, L. T.: Impacts of HONO sources on the photochemistry in Mexico City during the MCMA-2006/MILAGO Campaign, Atmos. Chem. Phys., 10, 6551-6567, doi:10.5194/acp-10-6551-2010, 2010.

Li, G., Bei, N., Tie, X., and Molina, L. T.: Aerosol effects on the photochemistry in Mexico City during MCMA-2006/MILAGRO campaign, Atmos. Chem. Phys., 11, 5169–5182, doi:10.5194/acp-11-5169-2011, 2011a.

Li, G., Zavala, M., Lei, W., Tsimpidi, A. P., Karydis, V. A., Pandis, S. N., Canagaratna, M. R., and Molina, L. T.: Simulations of organic aerosol concentrations in Mexico City using the WRF-CHEM model during the MCMA-2006/MILAGRO campaign, Atmos. Chem. Phys., 11, 3789–3809, doi:10.5194/acp-11-3789-2011, 2011b.

Li, M., Zhang, Q., Kurokawa, J. I., Woo, J. H., He, K., Lu, Z., Ohara, T., Song, Y., Streets, D. G., Carmicheal, G. R., Cheng, Y., Hong, C., Huo H., Jiang, X., Kang S., Liu, F., Su, H., and Zheng, B.: MIX: a mosaic Asian anthropogenic emission inventory under the international collaboration framework of the MICS-Asia and HTAP, Atmos. Chem. Phys., 17, 935-963, doi:10.5194/acp-17-935-2017, 2017.

Liggio, J., Li, S. M., and McLaren, R.: Reactive uptake of glyoxal by particulate matter, J. Geophys. Res.-

Atmos., 110, D10304, doi:10.1029/2004JD005113, 2005.
Moffet, R. C. and Prather, K. A.: In-situ measurements of the mixing state and optical properties of soot with implications for radiative forcing estimates, Proc. Natl. Acad. Sci. U.S.A., 106, 11872-11877, doi:10.1073/pnas.0900040106, 2009.
Morrison, H., Thompson, G., and Tatarskii, V.: Impact of cloud microphysics on the development of trailing stratiform precipitation in a simulated squall line: Comparison of one-and two-moment schemes, Mon. Weather Rev., 137, 991-1007, doi:10.1175/2008MWR2556.1, 2009.
Nenes, A., Pandis, S. N., and Pilinis, C.: ISORROPIA: A new thermodynamic equilibrium model for multiphase multicomponent inorganic aerosols, Aquat. Geochem., 4, 123-152, doi:10.1023/a:1009604003981, 1998.
Petters, M. D. and Kreidenweis, S. M.: A single parameter representation of hygroscopic growth and cloud condensation nucleus activity, Atmos. Chem. Phys., 7, 1961-1971, doi:10.5194/acp-7-1961-2007, 2007.
Petters, M. D. and Kreidenweis, S. M.: A single parameter representation of hygroscopic growth and cloud condensation nucleus activity–Part 2: Including solubility, Atmos. Chem. Phys., 8, 6273-6279. doi:10.5194/acp-8-6273-2008, 2008.
Petters, M. D. and Kreidenweis, S. M: A single parameter representation of hygroscopic growth and cloud condensation nucleus activity–Part 3: Including surfactant partitioning, Atmos. Chem. Phys., 13, 1081-1091, doi:10.5194/acp-13-1081-2013, 2013.
Phillips, V. T., DeMott, P. J., and Andronache, C.: An empirical parameterization of heterogeneous ice nucleation for multiple chemical species of aerosol. J. Atmos. Sci., 65, 2757-2783, doi:10.1175/2007JAS2546.1, 2008.
Phillips, V. T., Demott, P. J., Andronache, C., Pratt, K. A., Prather, K. A., Subramanian, R., and Twohy, C.: Improvements to an empirical parameterization of heterogeneous ice nucleation and its comparison with observations, J.Atmos. Sci., 70, 378-409, doi:10.1175/JAS-D-12-080.1, 2013.
Pruppacher, H. R. and Klett, J. D.: Microphysics of Clouds and Precipitation, Second Revised and Enlarged Edition with an Introduction to Cloud Chemistry and Cloud Electricity (Kluwer Academic Publishers, Reidel, Dordrecht, 954, 1997.
Khain, A. P.: Notes on state-of-the-art investigations of aerosol effects on precipitation: a critical review, Environ. Res. Lett., 4, 01500, doi:10.1088/1748-9326/4/1/015004, 2009.
Robinson, A. L., Donahue, N. M., Shrivastava, M. K., Weitkamp, E. A., Sage, A. M., Grieshop, A. P., Lane, T. E., Pierce, J. R., and Pandis, S. N.: Rethinking organic aerosols: Semivolatile emissions and photochemical aging, Science, 315, 1259-1262. doi:10.1126/science.1133061, 2007.
Shrivastava, M. K., Lane, T. E., Donahue, N. M., Pandis, S. N., and Robinson, A. L.: Effects of gas particle partitioning and aging of primary emissions on urban and regional organic aerosol concentrations, J. Geophys. Res.-Atmos., 113, D18301, doi:10.1029/2007jd009735, 2008.
Volkamer, R., San Martini, F., Molina, L. T., Salcedo, D., Jimenez, J. L., and Molina, M. J.: A missing sink for gas-phase glyoxal in Mexico City: Formation of secondary organic aerosol, Geophys. Res. Lett., 34, L19807, doi:10.1029/2007gl030752, 2007.
Wesely, M. L.: Parameterization of surface resistances to gaseous dry deposition in regional-scale numerical models, Atmos. Environ., 41, 52-63. https://doi.org/10.1016/j.atmosenv.2007.10.058, 2007.
Yau, M. K. and Rogers, R. R.: A short course in cloud physics (Pergamon, Tarrytown, New York). Elsevier, 1996.
Zhang, Q., Streets, D. G., Carmichael, G. R., He, K. B., Huo, H., Kannari, A., Kilimont, Z., Park, I. S., Reddy, S., Fu, J. S., Chen, D., Duan, L., Lei, Y., Wang, L. T., & Yao, Z. L.: Asian emissions in 2006 for the NASA INTEX-B mission, Atmos. Chem. Phys., 9, 5131-5153, doi:10.5194/acp-9-5131-2009, 2009.
Zhao, J., Levitt, N. P., Zhang, R., and Chen, J.: Heterogeneous reactions of methylglyoxal in acidic media: Implications for secondary organic aerosol formation, Environ. Sci. Techn., 40, 7682-7687, doi:10.1021/es060610k, 2006.
Zhou, X., Bei, N., Liu, H., Cao, J., Xing, L., Lei, W., Molina, L. T., and Li, G.: Aerosol effects on the development of cumulus clouds over the Tibetan Plateau, Atmos. Chem. Phys., 17, 7423-7434, doi:10.5194/acp-17-7423-2017, 2017.

Table S1. WRF-Chem model configurations

Domain	**Guanzhong Basin and its surrounding areas**
Simulation period	1200 UTC 23 to 1800 UTC 28, January 2022
Domain center	32.25°N, 119°E
Domain size	500 × 500
Horizontal resolution	6km × 6km
Meteorological boundary and initial conditions	NCEP 1°×1° reanalysis data
Chemical initial and boundary conditions	MOZART 6-hour output (Horowitz et al., 2003)
Cumulus scheme	None
Vertical resolution	51 vertical levels with a stretched vertical grid with spacing ranging from 30 m near the surface, to 400 m above 2.5 km
Microphysics scheme	Morrison two-moment scheme (Morrison et al., 2009)
Boundary layer scheme	MYJ TKE scheme (Janjić, 2001)
Surface layer scheme	MYJ surface scheme (Janjić, 2001)
Land-surface scheme	Unified Noah land-surface model (Chen and Dudhia, 2001)
Longwave radiation scheme	Goddard longwave scheme (Chou et al., 2001)
Shortwave radiation scheme	Goddard shortwave scheme (Chou and Suarez, 1999)
Chemical initial and boundary conditions	MOZART 6-hour output (Horowitz et al., 2003)
Anthropogenic emission inventory	2023 MEIC inventory (Geng et al., 2024)
Biogenic emission inventory	Online MEGAN model developed by Guenther et al. (2006)

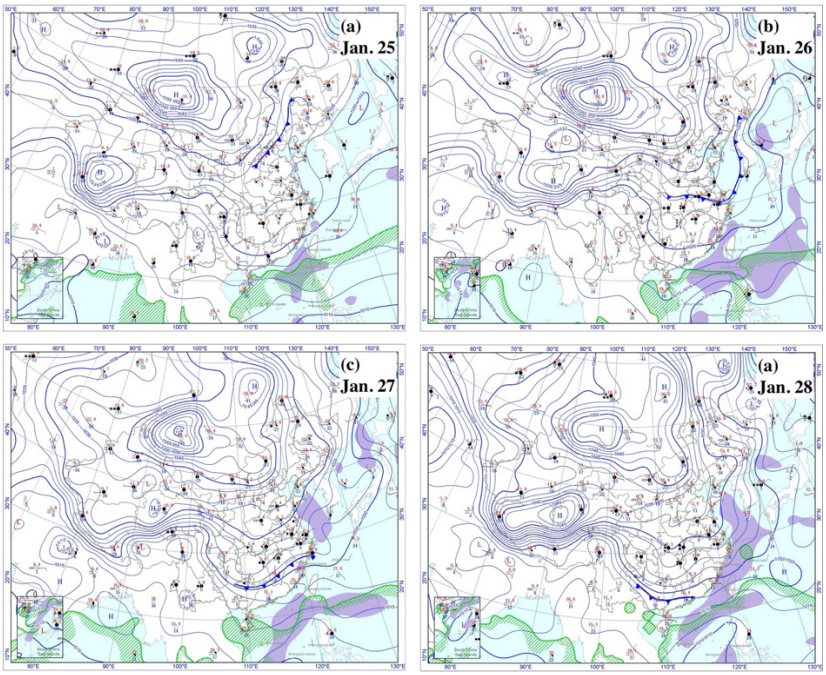

Figure S1: Synoptic situations on sea level pressure layer at 0800 LT from 25 to 28 January 2022.

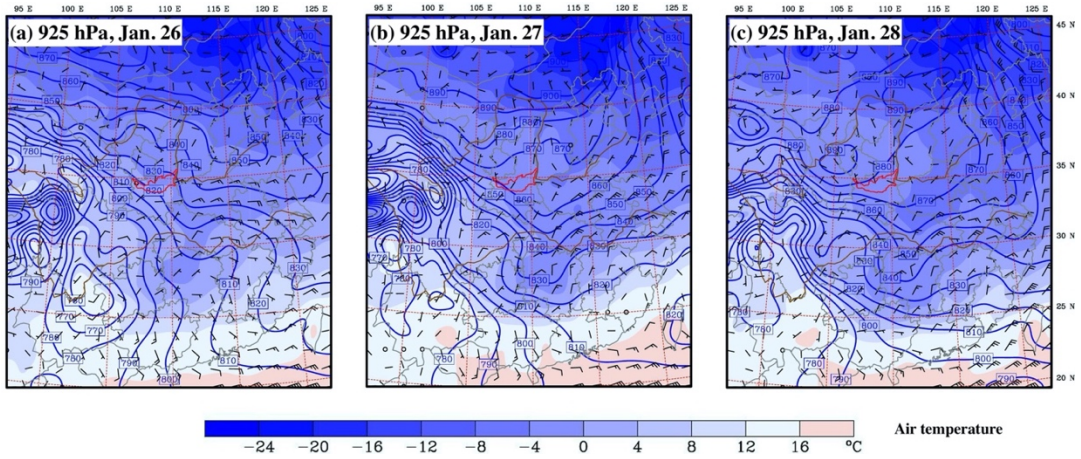

Figure S2: Synoptic situations at 925 hPa at 0000 UTC from 26 to 28 January 2022.

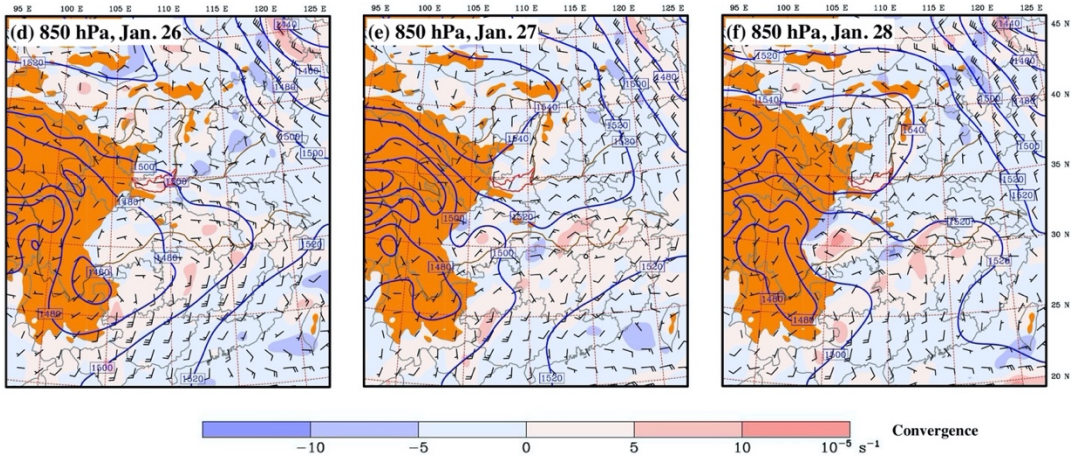

Figure S2: Continued for 850 hPa.

255

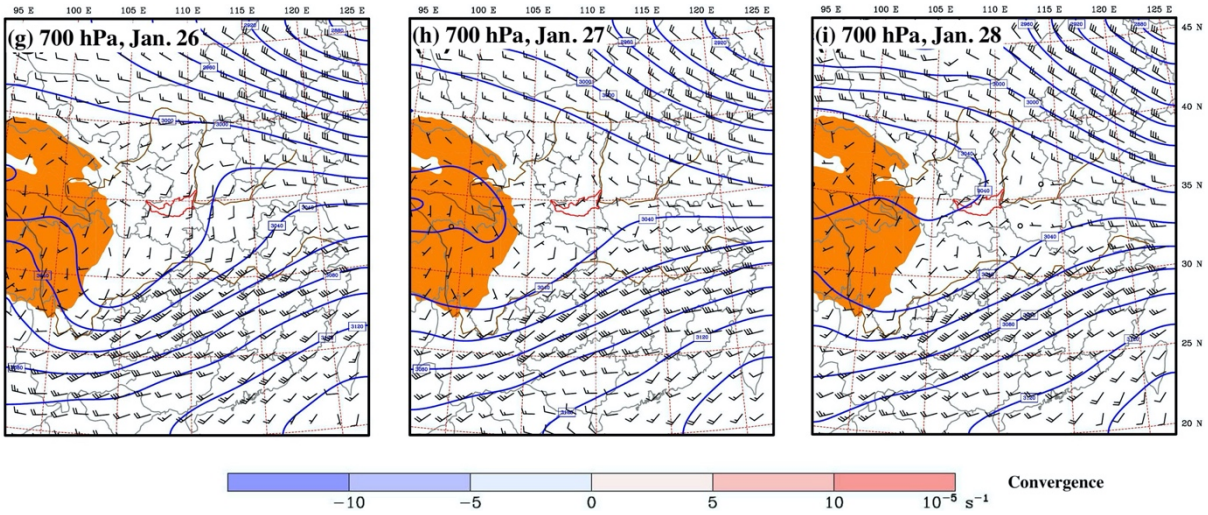

Figure S2: Continued for 700 hPa.

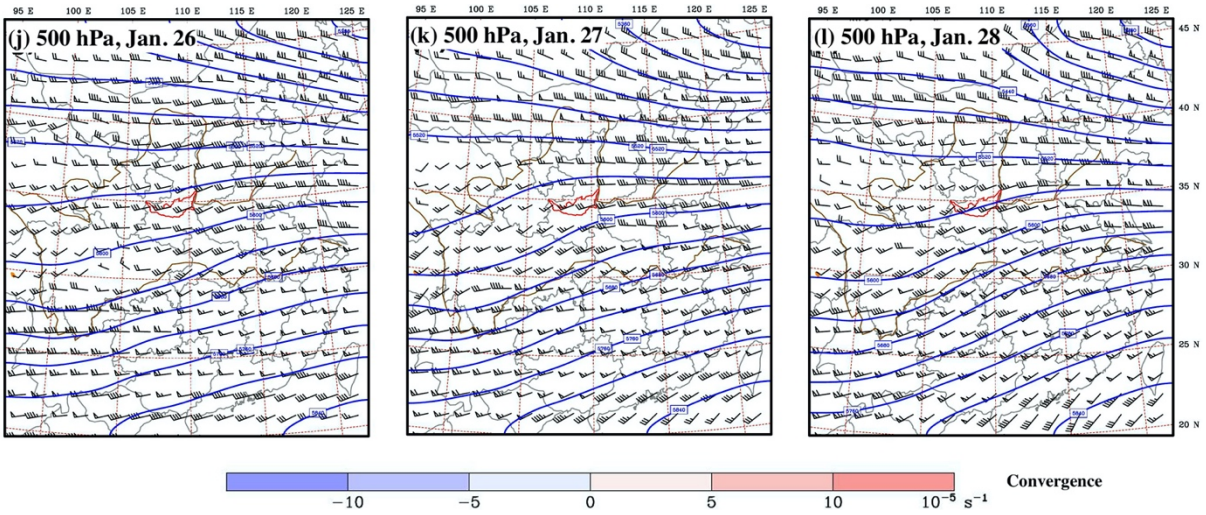

Figure S2: Continued for 500 hPa.

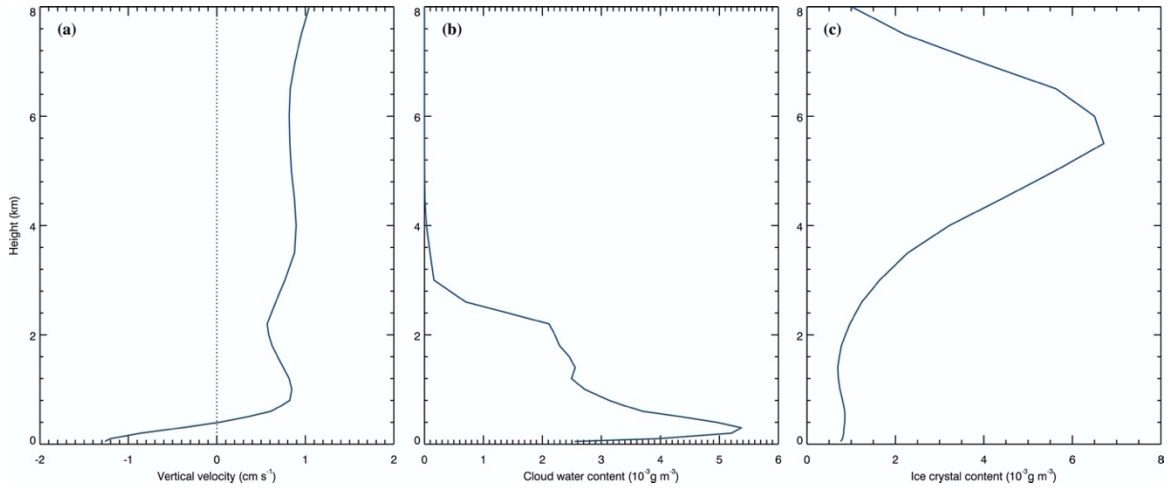

Figure S3: Profile of average (a) air temperature, (b) **cloud water content**, and (c) **ice water content** over GZB+GZBs from 26 to 28 January 2022.

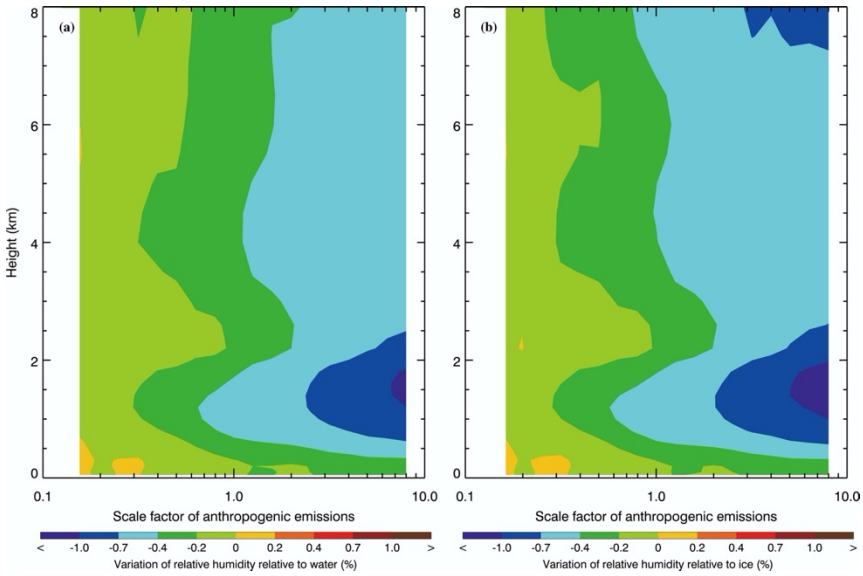

285

Figure S4: Profile variation of average **(a) RHW and (b) RHI due to ACIs in the F_ARI0** over GZB+GZBs from 26 to 28 January 2022**, with increasing** scale factor of anthropogenic emissions.

290

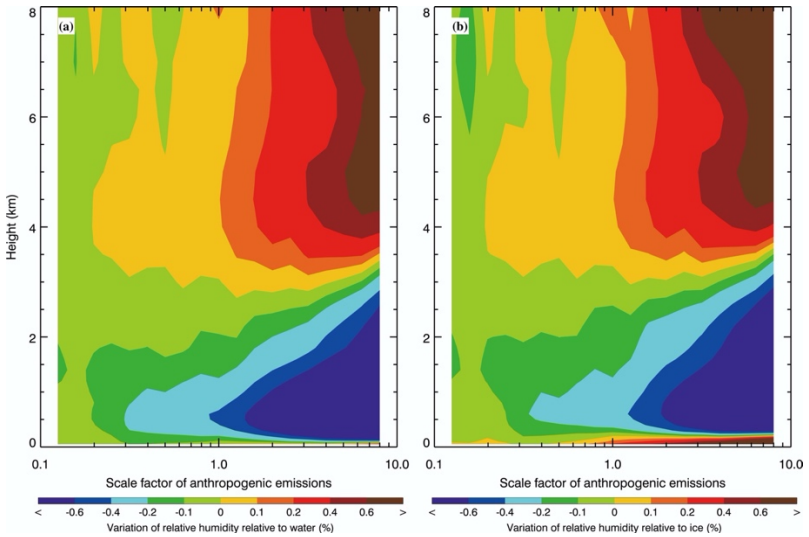

295 **Figure S5**: Profile variation of average (a) RHW, and (b) RHI over GZB+GZBs from 26 to 28 January 2022 caused by ARIs, as a function of the scale factor of anthropogenic emissions.

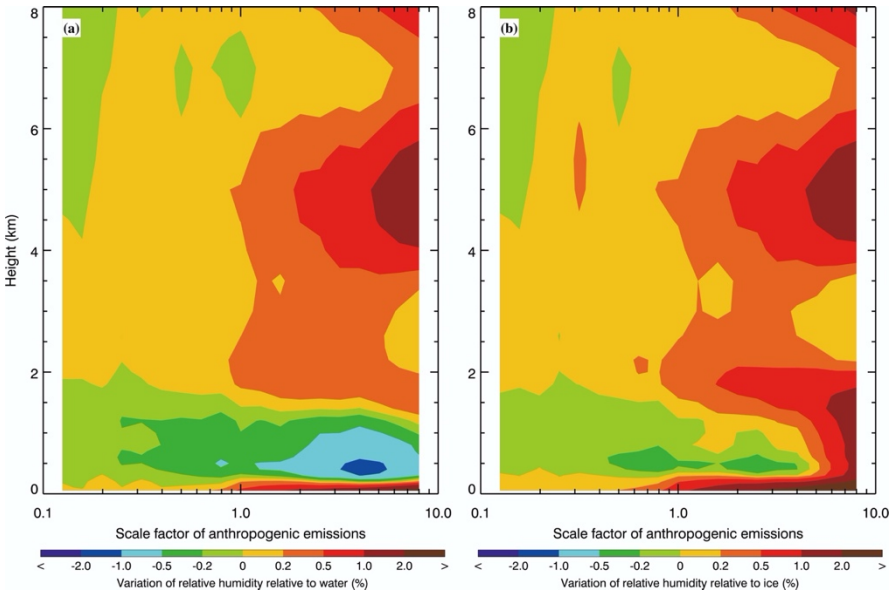

300

Figure S6: Profile variation of average (a) RHW, and (b) RHI over the GZB from 26 to 28 January 2022 caused by ARIs, as a function of the scale factor of anthropogenic emissions.

305

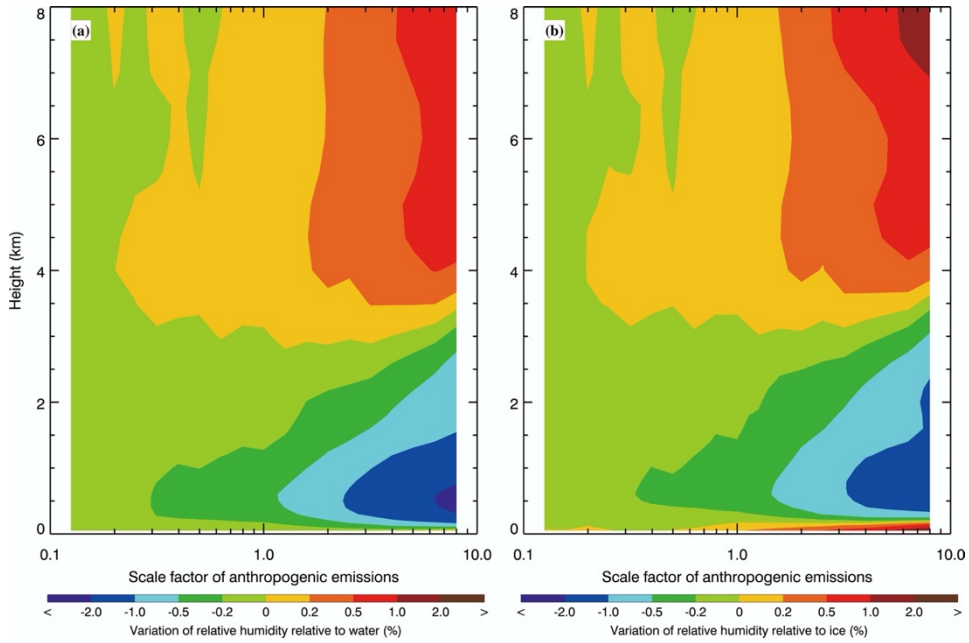

Figure S7: Profile variation of average (a) RHW, and (b) RHI over the GZBs from 26 to 28 January 2022 caused by ARIs, as a function of the scale factor of anthropogenic emissions.

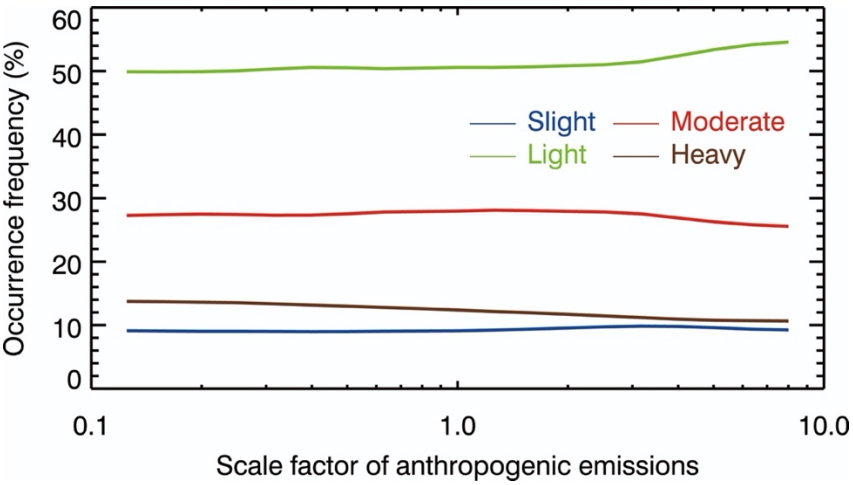

Figure S8: Variation of precipitation occurrence frequency over GZB+GZBs from 26 to 28 January 2022, as a function of the scale factor of anthropogenic emissions.